

## Article

# Structure Characteristics and Removal Behavior of the Deposited Carbon on Ni-Al<sub>2</sub>O<sub>3</sub> Catalyst for CO<sub>2</sub> Reforming of CH<sub>4</sub>

Wen-Long Mo <sup>1</sup>, Yuan Ren <sup>1</sup>, Yaya Ma <sup>1,2,\*</sup>, Jing Guo <sup>3,\*</sup>, Zhi-Hui Feng <sup>1</sup>, Shu-Pei Zhang <sup>4</sup> and Xiao-Qin Yang <sup>4</sup>

<sup>1</sup> State Key Laboratory of Chemistry and Utilization of Carbon Based Energy Resources, Key Laboratory of Coal Clean Conversion & Chemical Engineering Process (Xinjiang Uyghur Autonomous Region) and Key Laboratory of Oil and Gas Fine Chemicals of Ministry of Education, College of Chemical Engineering, Xinjiang University, Urumqi 830017, China; mowenlong@xju.edu.cn (W.-L.M.)

<sup>2</sup> Qingdao Institute of Bioenergy and Bioprocess Technology, Chinese Academy of Sciences, Qingdao 266101, China

<sup>3</sup> School of Chemistry and Chemical Engineering, Ningxia Normal University, Guyuan 756000, China

<sup>4</sup> Xinjiang Yihua Chemical Industry Co., Ltd., Changji 831700, China

\* Correspondence: mayy@qibebt.ac.cn (Y.M.); guojingsn@163.com (J.G.)

**Abstract:** Four catalysts were prepared in our previous work using the solution combustion method, incipient-wetness impregnation method, colloid mill circulating impregnation method, and hydrothermal-precipitation method, respectively, labeled as SCM, IMP, T310, and HTP. And the performance (stability) of the four catalysts for CO<sub>2</sub> reforming of CH<sub>4</sub> was investigated at 800 °C. In this paper, the composition and structure characteristics of the deposited carbon on the above four catalysts were tested through TEM, Raman, TPH, and TG-DTG technologies. The results showed that filamentous carbon was the primary type of carbon deposition on the catalysts, and a large amount of accumulated carbon would block the catalyst pores, affecting the catalytic performance. The carbon deposited on the catalyst prepared using the hydrothermal-precipitation method calcined at 800 °C exhibited a high degree of graphitization, and the proportion of graphitized carbon was considerable, which is harmful to the stability of the catalyst. The decarburization temperature of the deposited carbon on the four catalysts was mainly in the range of 500–700 °C. Using the Coats–Redfern model, as the reaction order was set as 1, 2, 3, 4, and 5, the decarburization activation energy ranged between 50 and 80 kJ/mol.

**Keywords:** CO<sub>2</sub> reforming of CH<sub>4</sub>; Ni-Al<sub>2</sub>O<sub>3</sub> catalyst; carbon deposition and removal



**Citation:** Mo, W.-L.; Ren, Y.; Ma, Y.; Guo, J.; Feng, Z.-H.; Zhang, S.-P.; Yang, X.-Q. Structure Characteristics and Removal Behavior of the Deposited Carbon on Ni-Al<sub>2</sub>O<sub>3</sub> Catalyst for CO<sub>2</sub> Reforming of CH<sub>4</sub>. *Processes* **2023**, *11*, 2968. <https://doi.org/10.3390/pr11102968>

Academic Editors: Davide Papurello, Guanghui Zhang, Jiawei Hu, Tianjia Chen, Jiawei Zhong and Qingxiang Ma

Received: 2 September 2023

Revised: 3 October 2023

Accepted: 9 October 2023

Published: 13 October 2023



**Copyright:** © 2023 by the authors. Licensee MDPI, Basel, Switzerland. This article is an open access article distributed under the terms and conditions of the Creative Commons Attribution (CC BY) license (<https://creativecommons.org/licenses/by/4.0/>).

## 1. Introduction

Massive emissions of CO<sub>2</sub> have become a major environmental problem. The extensive use of natural gas has resulted in the emission of large amounts of CH<sub>4</sub>. The utilization of the main GHGs, CO<sub>2</sub> and CH<sub>4</sub>, are extremely urgent. CO<sub>2</sub> reforming of CH<sub>4</sub> (CRM) can realize the direct conversion of the two gases, and it is of considerable importance for carbon emission reduction. The conversion of these two GHGs has attracted considerable attention all over the world [1–3]. In the CRM reaction, known as methane dry reforming (DRM), the H<sub>2</sub>/CO in the reaction product is close to 1, which can then produce liquid fuel and value-added chemicals via the Fischer–Tropsch process.

The choice of catalyst is important for the efficient and stable operation of CRM. Studies and practical applications indicate that Ni-based catalysts present high activity, good stability, and low cost. Moreover, they are widely used in industrial process, but these catalysts suffer from the problem of deactivation. Carbon deposition is one of the most important causes in carbon-related reaction processes. To date, the reaction mechanism of

carbon deposition is still being explored. Usually, the rate of carbon deposition depends on the rate of formation of carbon and its oxidation elimination rate [4].

Carbon deposition can be classified according to its morphology [5]. Amorphous carbon is highly reactive, and it can be eliminated using an oxidation reaction ( $C + O_2 = CO_2$ ) at 200–300 °C; polymeric carbon is composed of a partially hydrogenated carbon–carbon chain, with low reaction activity. It can be eliminated under appropriate conditions (e.g., in the presence of excess  $CO_2$ ). Graphitized carbon like the ring structure formed by six carbon atoms; it belongs to inert carbon deposition, which requires a high reaction temperature to be oxidized. Carbon nanotubes and filamentous carbon can seriously block the pores of the catalyst, resulting in a gradual decline in the activity of the used catalyst [6]. Du et al. [7] reported a CRM catalyst with a “limiting effect” and that can effectively inhibit carbon deposition. Huang et al. [8] prepared a Ni- $Al_2O_3$  catalyst modified by different promoters. The results showed that the high dispersion of Ni and Ca on the surface of the catalyst caused the reforming performance to be enhanced; moreover, the carbon deposition on the surface of Co-Ni- $Al_2O_3$  was primarily to be filamentous one.

TEM images of the HTP and IMP catalysts before and after the reforming reaction are provided in Reference [9]. Filamentous carbon was found on the surface of the catalyst, and a large accumulation of this species will block the pore of the catalyst. However, Reference [9] neither focuses on the amount, composition, or structure characteristics of the carbon deposition nor discusses its elimination strategy. Based on the previous work, this paper focuses on the composition distribution and structure characteristics of carbon deposition on the catalyst surface after the stability test. Furthermore, the elimination rule of carbon deposition will be analyzed, providing a theoretical reference for extending the service life of the catalyst.

## 2. Carbon Deposition on Different Ni-Based Catalysts

Four catalysts, SCM, IMP, T310, and HTP, were prepared, and Reference [9] provides the methods for the preparation of the said catalysts. Performance of the four catalysts was also investigated at 800 °C in our previous work [9].

Moreover, the data in Reference [9] reflect the change of  $CH_4$  conversion of the above catalysts. Within 10 h, the  $CH_4$  conversion of HTP is ~85%, that of T310 is ~78%, while that of IMP and SCM are about 75% and 70%, respectively. With increase in the reaction time, however, the  $CH_4$  conversion of HTP and T310 rapidly decreases to 50% after 60 and 80 h, respectively; while the stability of IMP and SCM is better, with  $CH_4$  conversion decreasing to 50% after reaction for 100 and 92 h, respectively.

### 2.1. Catalyst Characterization

#### 2.1.1. Transmission Electron Microscope (TEM)

Size of loaded Ni particles was directly observed using the Tecnai G220 Stw from the American FEI company, Hillsboro, OR, USA. The acceleration voltage was 200 kV, and the sample was subjected to ultrasonic dispersion in anhydrous ethanol before testing.

#### 2.1.2. Thermogravimetry (TG-DTG)

Thermogravimetry was used to test the deposited carbon on the surface of catalyst. SDTQ-600 instrument from TA Company (Boston, MA, USA) was introduced to analyze the deposited carbon. The maximum temperature was set at 1000 °C with heating rate of 10 °C/min (air, 100 mL/min).

#### 2.1.3. Raman

Raman spectra of the used catalyst were obtained using a SENTERRA Raman microscope from Bruker (Billerica, MA, USA).

#### 2.1.4. Temperature-Programmed Hydrogenation (TPH)

Through TPH technology, carbon deposition on the catalyst can be tested, which was conducted on a Chem-BET pulse TPR/TPD instrument from Kanta Company, with a catalyst dosage of 50 mg. The sample was firstly pre-treated at 673 K in He flow for 1 h, and then switched to a mixture of 5% H<sub>2</sub> + 95% Ar with the flow rate of 100 mL/min, and the temperature was heated to 1273 K with the heating rate of 10 °C/min.

#### 2.2. Spectroscopic Characteristics of the Carbon Deposition (Raman)

Raman spectroscopy was performed (Figure 1). As can be evidenced from Figure 1, there are two obvious peaks at ~1338 and 1570 cm<sup>-1</sup>. The first peak, the D band, is attributed to carbon species with an amorphous structure; the second peak, the G band, corresponds to highly symmetrical and ordered graphitized carbon species [10,11]. Intensities of the D and G bands are considerably lower in SCM and IMP, indicating that the amount of deposited carbon on SCM and IMP is small.

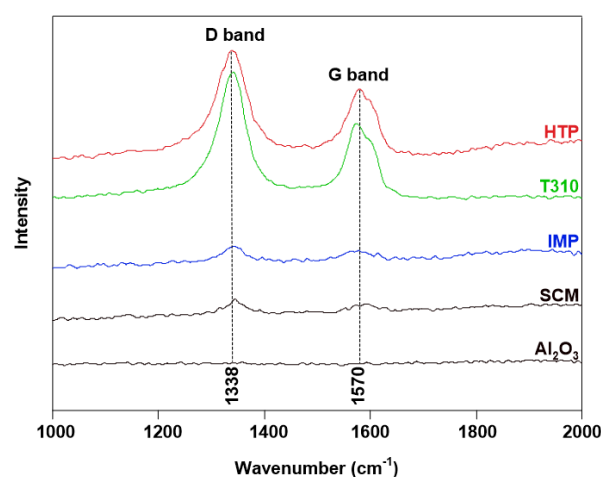


**Figure 1.** Raman spectra of the endurance-tested catalysts.

The ratio of the D and G bands ( $I_D/I_G$ ) has been reported to reflect the degree of formation of graphitized carbon species, i.e., the degree of graphitization. The lower the value for this ratio, the higher the degree of graphitization of the carbon species [11,12]. Based on the data reported in Figure 1, the  $I_D/I_G$  values for the four catalysts are calculated (Table 1). Table 1 shows that the  $I_D/I_G$  value for each sample is >1.00, which indicates that the content of D carbon is higher than that of G carbon, and the graphitization degree of surface carbon of each sample is lower. Furthermore, the  $I_D/I_G$  value of HTP and T310 is about 1.8, showing that the degree of graphitization is lower, i.e., there are many disordered carbon species on the surface. It is worth noting that the  $I_D/I_G$  values of SCM and IMP are lower, while the average carbon deposition rate is also low (<1.00 mg/(g<sub>cat</sub>·h)), i.e., the total content of graphitized carbon is relatively low, resulting in the better stability of both. And the total carbon deposition on HTP and T310 is large, resulting in a potentially high absolute content of graphitized carbon.

**Table 1.** Raman spectroscopy data for the stability-tested catalysts.

| Catalyst | Average Carbon Formation Rate (mg/g <sub>cat</sub> ·h) | Intensity Ratio of D and G Bands of the Raman Spectra ( $I_D/I_G$ ) |
|----------|--|---|
| SCM      | 0.98   | 1.25  |
| IMP      | 0.88   | 1.32  |
| T310     | 3.05   | 1.85  |
| HTP      | 5.49   | 1.78  |

### 2.3. Hydrogenation Activity of Carbon Deposition (TPH)

TPH characterization of the carbon deposition was performed (Figure 2). Figure 2 shows that there are three types of obvious surface hydrogenation peaks in each sample [11]. Before 350 °C, the first peak is attributed to  $\alpha$ -type carbon, which is also the expected carbon deposition type during reforming reaction. At a high temperature, this type of carbon is easily converted to less active carbon species: the  $\beta$ -type carbon. The second hydrogenation peak, appearing in 350–550 °C, is attributed to  $\beta$ -type carbon species, which easily deposits in the catalyst pores or enters the lattice of the active component-Ni; moreover, the  $\beta$ -type carbon presents certain activity. After long-term accumulation at a high temperature, the carbon is easily converted to the inert  $\gamma$ -type carbon species. After 550 °C, the third type of hydrogenation peak is observed, which belongs to  $\gamma$ -type carbon, such as graphitized carbon. The  $\gamma$ -type carbon is difficult to eliminate via hydrogenation at a high temperature. Figure 2 shows that the type of carbon deposition is mainly a filamentous one, which is consistent with the results of the subsequent TG-DTG experiments. Because of the large amount of carbon deposited on HTP and T310, some of the carbon deposition might convert to the  $\gamma$ -type carbon. The low-temperature hydrogen consumption peaks are primarily observed at ~200–300 °C, which are attributed to surface amorphous carbon and channel amorphous carbon, respectively.

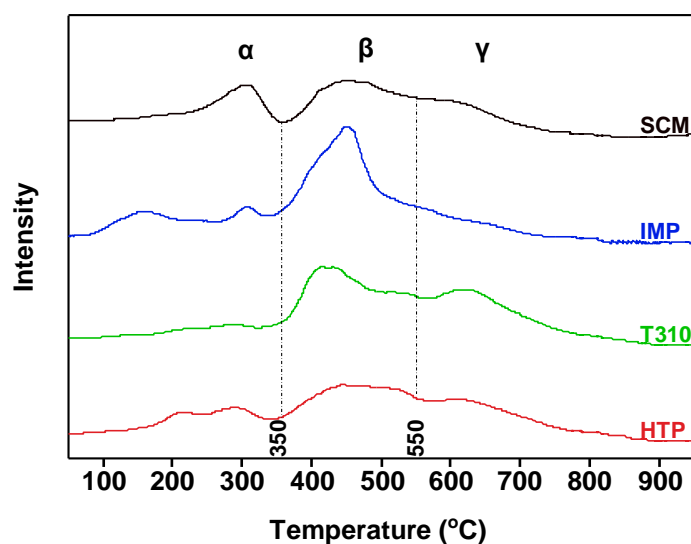


**Figure 2.** Results of TPH experiments for the stability-tested catalysts.

Origin software (version Origin 2021) was used to analyze the area ratio of each peak from TPH profiles of the four used catalysts (Table 2). Before 350 °C, the first type of hydrogenation peak ( $\alpha$ -type) can be observed. The area proportions of the first hydrogen consumption peaks of SCM and HTP at low temperatures (<350 °C) account for 30–35%, higher than those of IMP and T310. Moreover, the area proportion of T310 is as low as 9.79%, indicating that there is more inert carbon on this catalyst. The proportion of  $\beta$ -type carbon, the main type of deposited carbon, in each catalyst is in the range of 55–80%, demonstrating that the surface carbon deposition on each catalyst is primarily composed of filamentous carbon or coated carbon. With respect to  $\gamma$ -type carbon species, both T310 and HTP account for a high proportion, and their decarburization behavior directly affects the stability of the catalysts.

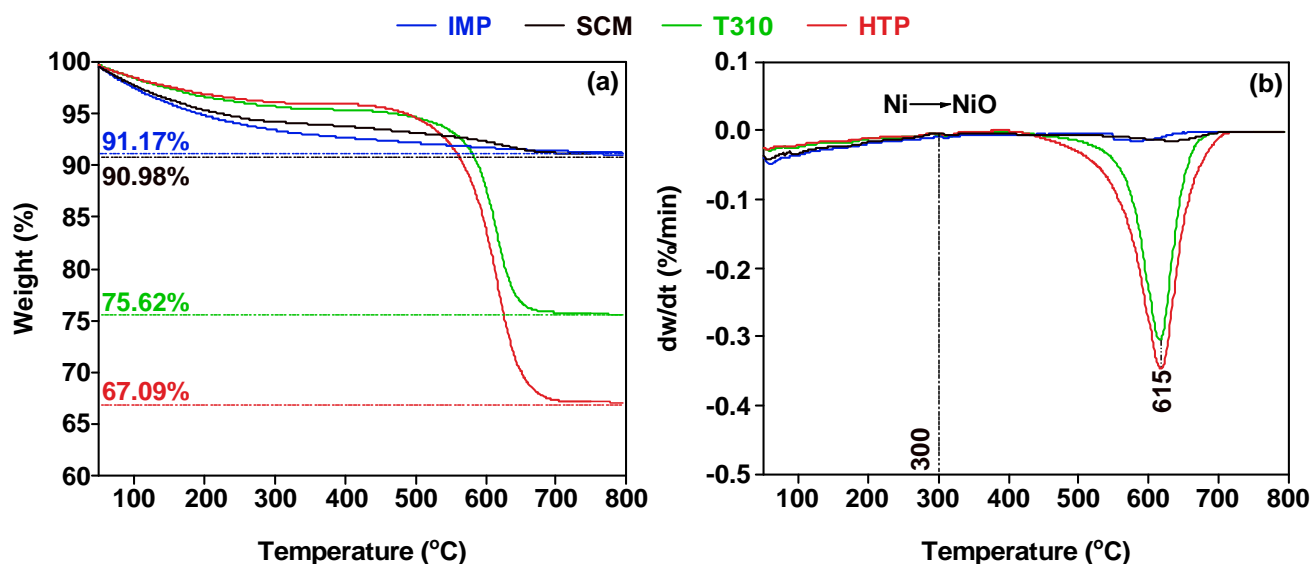
**Table 2.** Proportion of the area of each hydrogenation peak due to different carbon species for the stability-tested catalysts.

| Catalyst | $\alpha$ -Type Carbon (%) | $\beta$ -Type Carbon (%) | $\gamma$ -Type Carbon (%) |
|----------|---------------------------|--------------------------|---------------------------|
| SCM      | 35.52                     | 56.13                    | 8.35                      |
| IMP      | 19.02                     | 77.65                    | 3.33                      |
| T310     | 9.79                      | 64.85                    | 25.36                     |
| HTP      | 31.15                     | 54.82                    | 14.03                     |

#### 2.4. Weight Loss Behavior of Carbon Deposition (TG-DTG)

##### TG-DTG Analysis

TG-DTG analysis performed for each catalyst after the stability test are provided in Figure 3. As can be evinced from Figure 3a, the TG profile of each catalyst is quite different from one another, indicating that the carbon deposition process was different, particularly with respect to the mass of carbon deposition. The weight losses observed for HTP and T310 are high at 32.91% and 24.38%, respectively. While the carbon deposition of SCM and IMP are lower at 9.02% and 8.83%, respectively. As reported from Figure 3b, a small weight loss rate peak can be observed for each catalyst at  $\sim 300$  °C; this peak is attributed to the oxidation of the active component Ni (the oxidation product is NiO). Furthermore, a strong weight-loss rate peak for HTP and T310 is detected at 615 °C; this observation indicates that the deposited carbon on T310 and HTP was primarily composed of filamentous carbon, which is characterized by a low reactivity; in fact, the accumulation of this type of carbon in large amounts would block the catalyst channels, causing a rise in the bed pressure drop, thus affecting catalyst performance [12]. Importantly, this type of carbon can only be removed via a reaction with  $H_2$ , CO, and  $O_2$  at a high temperature.

**Figure 3.** TG (a) and DTG (b) profiles of the endurance-tested catalysts.

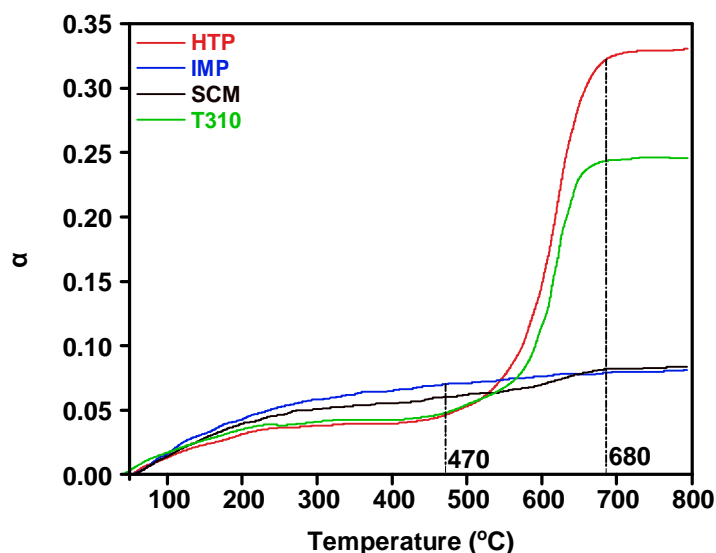
The time-average carbon deposition rates with the catalytic reaction processes are calculated based on the data in Figure 3a (Table 3). As can be seen from this table, the carbon deposition rates vary greatly for each sample. In particular, the carbon deposition rates measured for SCM and IMP are lower than  $1.00 \text{ mg}/(\text{h}\cdot\text{g}_{\text{cat}})$ , and the values of T310 and HTP are high at  $3.05$  and  $5.49 \text{ mg}/(\text{h}\cdot\text{g}_{\text{cat}})$ .

**Table 3.** Weight loss, reaction time, and carbon deposition rate for the stability-tested catalysts.

| Catalyst | Weight Loss (%) | Reaction Time (h) | Carbon Deposition Rate (mg/(h·g <sub>cat</sub> )) |
|----------|-----------------|-------------------|---|
| SCM      | 9.02            | 92                | 0.98  |
| IMP      | 8.83            | 100               | 0.88  |
| T310     | 24.38           | 80                | 3.05  |
| HTP      | 32.91           | 60                | 5.49  |

### 2.5. Coats–Redfern Model for Carbon Elimination Kinetics

According to reference [13], the effect of temperature on carbon removal conversion for IMP, SCM, T310, and HTP is reflected in Figure 4. As can be inferred from Figure 4, the carbon removal process could be divided into three stages: one occurring in the low temperature region (<470 °C), one at mid-range temperatures (470–680 °C), and one in the high temperature range (>680 °C). In the low-temperature region (<470 °C), the conversion rate exhibits little change as the temperature increases. In the second stage (470–680 °C), the temperature presents a considerable impact on the carbon conversion of HTP and T310, indicating that the carbon removal process of the two catalysts mainly takes place in the 470–680 °C range. In the high-temperature region (>680 °C), the effect of temperature on the carbon conversion gradually decreases and the curve tends to be flat.

**Figure 4.** Conversion-temperature profiles for the decarburization of the four catalysts.

According to the Coats–Redfern model, as the reaction order  $n$  is selected as 1, 2, 3, 4, and 5, the decarburization kinetics of HTP and T310 in the second stage (470–680 °C) are fitted, and the results are reported in Figure 5 and Table 4. As can be seen in Table 4, when  $n = 1$ , the  $2RT/E$  value tends to 0, and the  $R^2$  value tends to 1; in other words, the Coats–Redfern model is applicable to the simulation of the carbon removal process.

As can be observed from Table 4, the  $R^2$  value for T310 decreases as the reaction order increases. Indeed, a better fitting effect for the sample is achieved as  $n = 1$  ( $R^2 = 0.9433$ ), with the decarburization activation energy of 56.49 kJ/mol. And the fitting effect of HTP is better when  $n = 2$ , with  $R^2$  of 0.9389. As can be evinced from the data in Table 4, the activation energy for the decarburization of HTP increases more obviously with the increase in  $n$ , which may be due to the higher the value of  $n$ , the more complex the decarburization reaction process. Combining the assumption that  $2RT/E$  tends to 0 and the  $R^2$  value tends to 1, the experimental data on the decarburization of HTP are fitted more suitably as  $n = 2$ , and the activation energy is 62.13 kJ/mol.

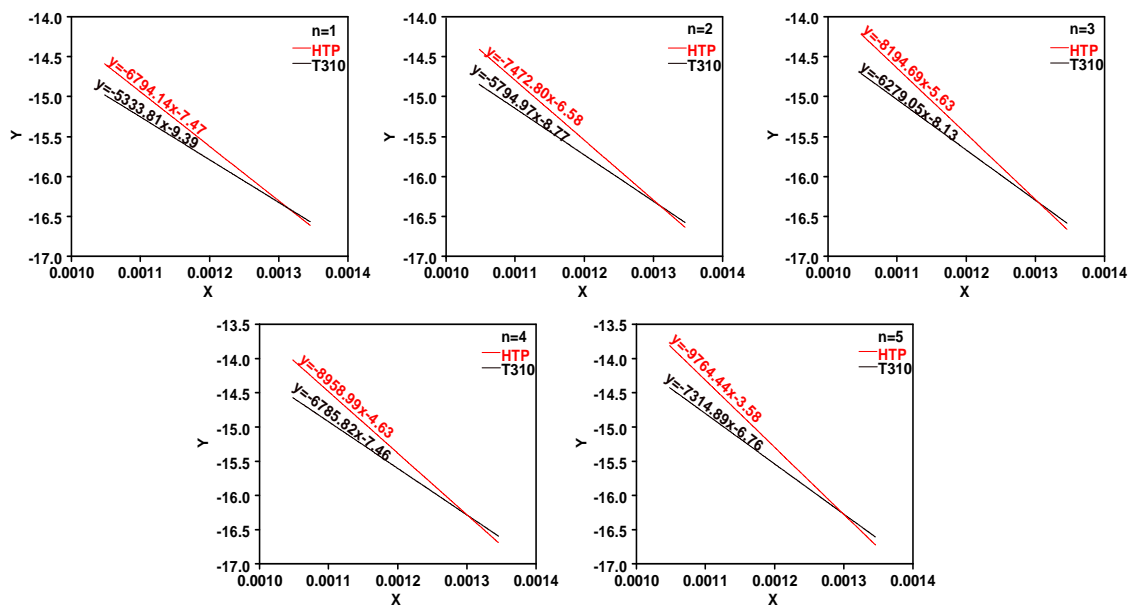


Figure 5. Kinetic fitting results for the decarburization of T310 and HTP. n: reaction order.

Table 4. Carbon removal kinetic parameters for the carbon deposited on T310 and HTP catalysts in 470–680 °C range.

| n | Catalyst | Regression Equation    | Correlation Coefficient ( $R^2$ ) | Activation Energy (E, kJ/mol) | Pre-Exponential Factor (A, $\text{min}^{-1}$ ) | 2RT/E  |
|---|----------|------------------------|-----------------------------------|-------------------------------|--|--------|
| 1 | T310     | $y = -6794.14x - 7.47$ | 0.9433                            | 56.49                         | 38.75  | 0.1384 |
|   | HTP      | $y = -5333.81x - 9.39$ | 0.8649                            | 44.35                         | 4.46   | 0.1762 |
| 2 | T310     | $y = -5794.97x - 8.77$ | 0.8633                            | 48.18                         | 9.01   | 0.1622 |
|   | HTP      | $y = -7472.80x - 6.58$ | 0.9389                            | 62.13                         | $1.04 \times 10^{-2}$                          | 0.1258 |
| 3 | T310     | $y = -6279.05x - 8.13$ | 0.8615                            | 52.20                         | 18.51  | 0.1497 |
|   | HTP      | $y = -8194.69x - 5.63$ | 0.9341                            | 68.13                         | $2.94 \times 10^{-2}$                          | 0.1147 |
| 4 | T310     | $y = -6785.82x - 7.46$ | 0.8596                            | 56.42                         | 39.09  | 0.1385 |
|   | HTP      | $y = -8958.99x - 4.63$ | 0.9291                            | 74.49                         | $8.74 \times 10^{-2}$                          | 0.1049 |
| 5 | T310     | $y = -7314.89x - 6.76$ | 0.8576                            | 60.82                         | 84.86  | 0.1285 |
|   | HTP      | $y = -9764.44x - 3.58$ | 0.9240                            | 81.18                         | $2.72 \times 10^3$                             | 0.0963 |

### 3. Deposited Carbon on HTP

Calcination temperatures of the used catalysts were prepared using the hydrothermal-precipitation method at 500 °C and 800 °C, and the catalysts were marked as cat-500 and cat-800. Reference [14] presents the catalyst preparation method.

Reference [14] also gives the stability test results for cat-500 and cat-800. During the 112 h experiment, cat-800 exhibited higher activity, with  $\text{CO}_2$  conversion remaining around 95% and a deactivation rate of 0.0536 point/h. And the activity of cat-500 was lower, with  $\text{CO}_2$  conversion decreasing from 80% at the beginning to 60% at the end of the reaction (112 h), and a deactivation rate which was much higher (0.154 point/h) than for cat-800.

#### 3.1. Surface Morphology of the Carbon Deposition (TEM Characterization)

Figure 6 shows TEM images of cat-500 and cat-800 after the stability test. As can be observed from Figure 6, the carbon is mainly amorphous and filamentous with a diameter of less than 10 nm, which is consistent with the results of the subsequent Raman and TG-DTG analyses.

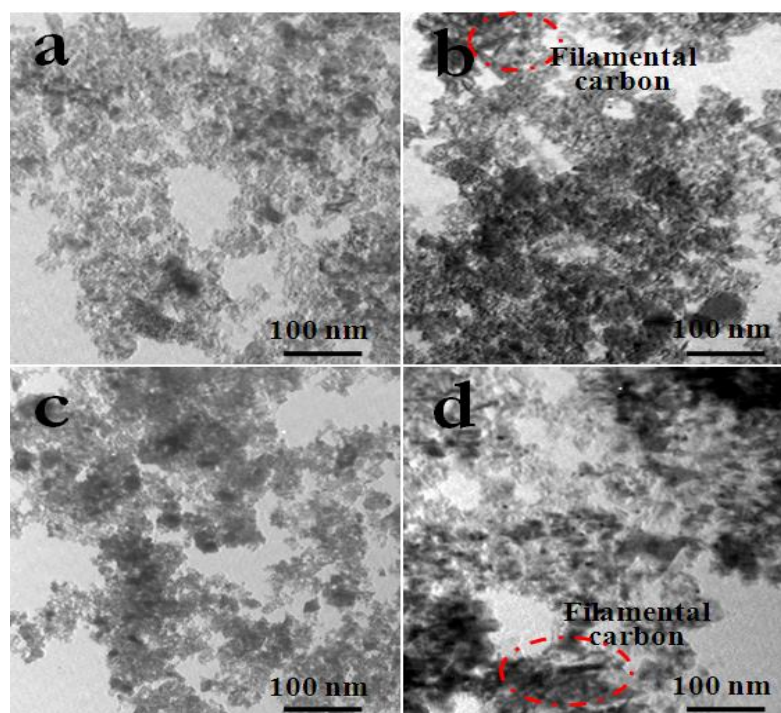


**Figure 6.** TEM results of the catalysts (cat-500 before (a) and after (b) reaction; cat-800 before (c) and after (d) reaction).

Average size of Ni before and after the reaction is estimated based on the TEM diagrams (Table 5). Table 5 indicates that the size of Ni in cat-500 was 12.9 nm before the reaction and increased to 23.5 nm after the reaction, representing an 82.17% increase. The size of Ni in cat-800 after the reaction was 12.0 nm, which is only a 48.15% increase over its pre-reaction size, and about half that of cat-500. Therefore, cat-800 exhibits a stronger anti-sintering ability than cat-500, which might be an important reason for its better stability.

**Table 5.** Ni size of cat-500 and cat-800 before and after the reaction.

| Catalyst | Ni Size (nm)        |                    | Increasing Rate (%) |
|----------|---------------------|--------------------|---------------------|
|          | Before the Reaction | After the Reaction |                     |
| cat-500  | 12.9                | 23.5               | 82.17               |
| cat-800  | 8.1                 | 12.0               | 48.15               |

### 3.2. Spectral Characteristics of Carbon Deposition (Raman Spectroscopy Characterization)

Raman spectroscopy was used to characterize the samples, and the obtained profiles are presented in Figure 7. As depicted in Figure 7, before the reaction, no signal was observed in  $1000\text{--}2000\text{ cm}^{-1}$  of the Raman spectra for both cat-500 and cat-800. After the reaction, there were significant Raman peaks, and one is the D band at  $1338\text{ cm}^{-1}$  attributed to amorphous carbon and another is the G band attributed to graphitized carbon at  $1570\text{ cm}^{-1}$ . On the one hand, the intensity of the D and G bands of cat-500 is significantly higher than that of cat-800, which means that the surface of cat-500 shows a larger amount of deposited carbon, which is consistent with the TG-DTG analysis results. On the other hand, the value of intensity ratio ( $I_D/I_G$ ) from the D and G bands of the two samples is quite different, 2.2 for cat-500 and 1.0 for cat-800, indicating that the catalyst prepared with the calcination temperature of  $800\text{ }^\circ\text{C}$  presents a higher degree of graphitization after the reaction. Graphitized carbon is inactive, which is not conducive to catalyst stability. Fortunately, the total carbon deposition on cat-800 is small, demonstrating that the total content of graphitized carbon is relatively low, and the catalyst activity is not significantly reduced within the 110 h of the experiment range.

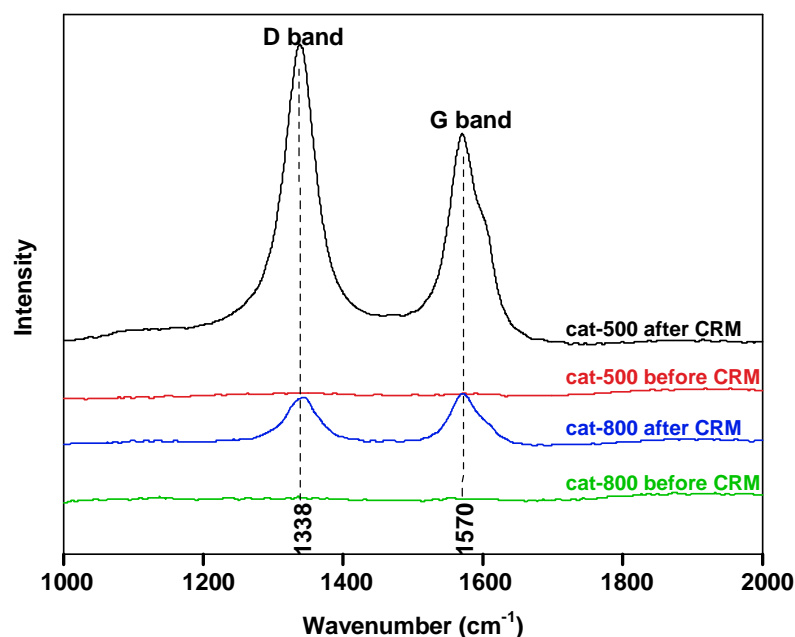


Figure 7. Raman spectra of the endurance-tested Ni-based catalysts.

### 3.3. Weight Loss Behavior of Carbon Deposition (TG-DTG Characterization)

Figure 8 reported the results of the TG-DTG characterization of cat-500 and cat-800 catalysts after the life test. A large amount of carbon is deposited on the cat-500 and cat-800 catalysts. However, the catalyst activity, especially for cat-800, does not exhibit a significant decrease.

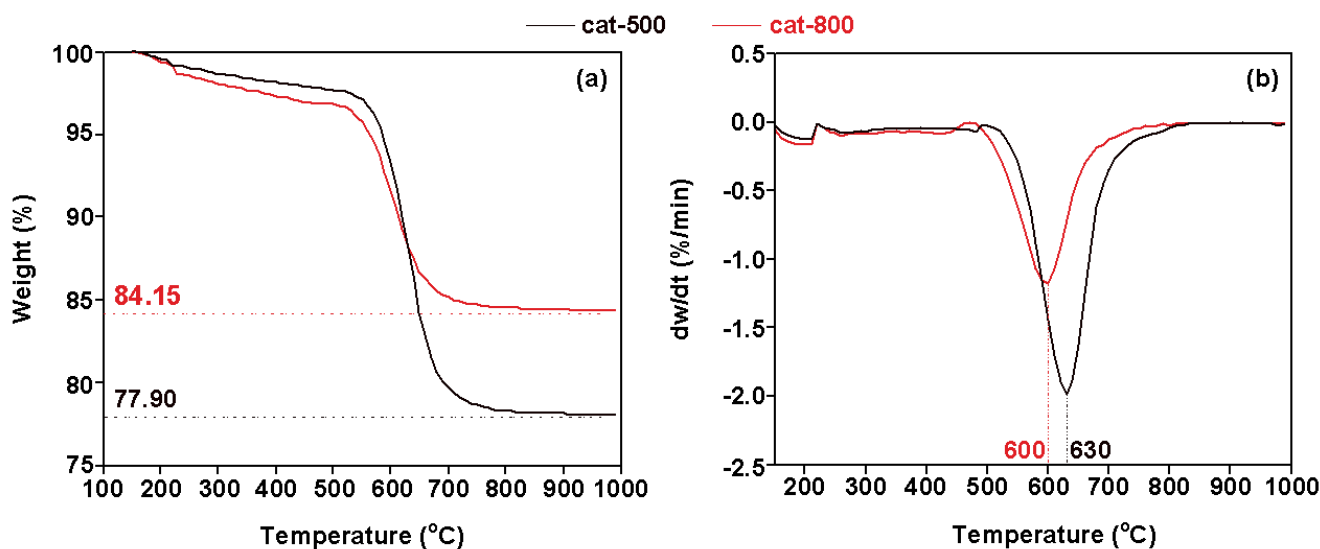


Figure 8. TG (a) and DTG (b) results of the used catalysts.

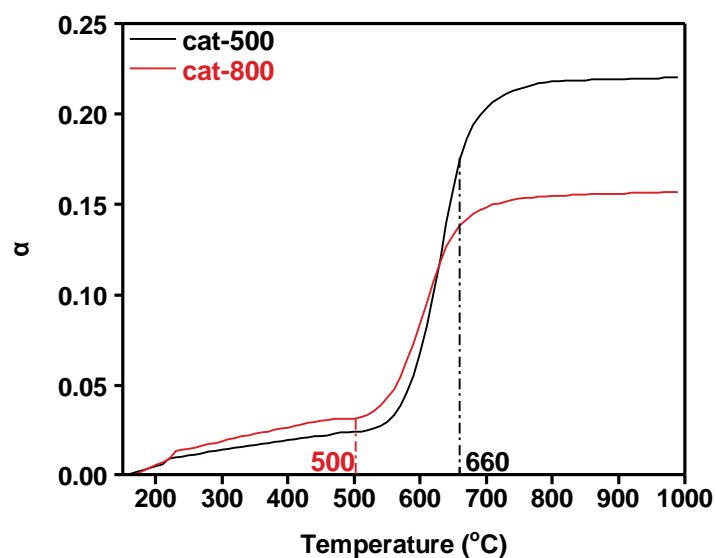
It can be seen from Figure 8 that, firstly, both samples exhibit a large weight-loss rate peak at about 600–630 °C, which can be classified as filamentous carbon. Secondly, the amount of carbon deposition of cat-500 and cat-800 is 22.10% and 15.85%, respectively. The average carbon deposition rates for the two catalysts over the 112 h life test was calculated based on these data (Table 6). As can be observed from the table, the carbon deposition rate is only 1.42 mg/(h·g<sub>cat</sub>) for cat-800, lower than the rate of cat-500.

**Table 6.** Average carbon deposition rates of cat-500 and cat-800.

| Catalyst | Weight Loss (%) | Reaction Time (h) | Average Carbon Deposition Rate (mg/(h·g <sub>cat</sub> )) |
|----------|-----------------|-------------------|---|
| cat-500  | 22.10           | 112               | 1.97  |
| cat-800  | 15.85           |                   | 1.42  |

### 3.4. Carbon Elimination Kinetics Based on Coats–Redfern Model

The effect of temperature on the carbon removal behavior of cat-500 and cat-800 is reflected in Figure 9, which is derived from Figure 8. The carbon removal process could be divided into three periods: 150–500 °C, 500–660 °C, and 660–990 °C. In the low-temperature part (<500 °C), the carbon conversion rate changes little as the temperature increases. In the second stage (500–660 °C), temperature shows a significant impact on the carbon conversion reaction ( $C + O_2 = CO_2$ ) for both cat-500 and cat-800, such that the conversion profiles change significantly as a function of temperature, indicating that the decarbonization reaction of the above two catalysts occurs primarily in the 500–660 °C region. In the >660 range, the effect of temperature on decarburization gradually decreases, and the carbon conversion-temperature profiles tend toward stability.

**Figure 9.** Carbon conversion-temperature relationship of cat-500 and cat-800.

Based on Coats–Redfern model, the kinetics of decarburization of cat-500 and cat-800 are fitted in the second stage (500–660 °C), and the reaction order is selected as  $n = 1–5$  (Figure 10 and Table 7).

As can be seen in Table 7, the  $R^2$  values obtained for cat-500 and cat-800 decrease as the value of  $n$  increases. When  $n = 1$ , the goodness of the fitting effect is better with  $R^2$  of 0.9118 for cat-500 and 0.9642 for cat-800. Furthermore, the activation energy of cat-500 and cat-800 increases with the reaction order, presumably because the higher the reaction order, the more complex the simulated decarburization reaction process. Combining the assumption that  $2RT/E$  tends to 0 and  $R^2$  tends to 1, the kinetic data for cat-500 and cat-800 decarburization are better fitted when a value of 1 is imposed for the reaction order  $n$ . In this context, the decarburization activation energy is 71.87 kJ/mol for cat-500 and 52.41 kJ/mol for cat-800.

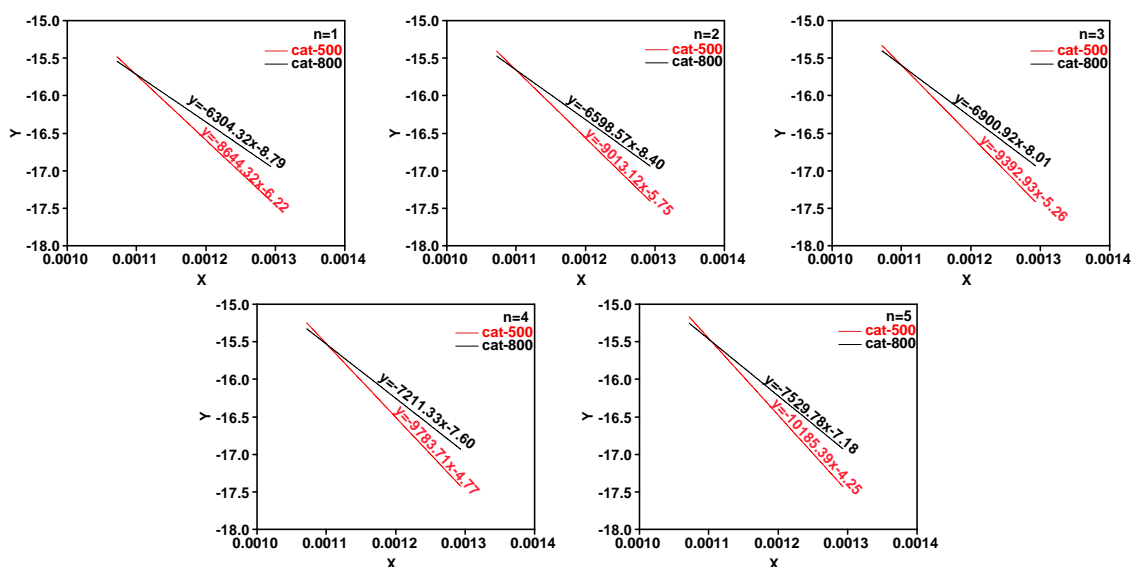


Figure 10. Kinetic fitting results of cat-500 and cat-800. n: reaction order.

Table 7. Carbon removal kinetic parameters for cat-500 and cat-800 in the 500–660 °C range.

| n | Catalyst | Regression Equation      | Correlation Coefficient ( $R^2$ ) | Activation Energy (E; kJ/mol) | Pre-Exponential Factor (A; $\text{min}^{-1}$ ) | 2RT/E  |
|---|----------|--------------------------|-----------------------------------|-------------------------------|--|--------|
| 1 | cat-500  | $y = -8644.32x - 6.22$   | 0.9118                            | 71.87                         | $1.72 \times 10^2$                             | 0.1157 |
|   | cat-800  | $y = -6304.32x - 8.79$   | 0.9642                            | 52.41                         | 9.61   | 0.1586 |
| 2 | cat-500  | $y = -9013.12x - 5.75$   | 0.9093                            | 74.94                         | $2.87 \times 10^2$                             | 0.1109 |
|   | cat-800  | $y = -6598.57x - 8.40$   | 0.9637                            | 54.86                         | 14.85  | 0.1515 |
| 3 | cat-500  | $y = -9392.93x - 5.26$   | 0.9067                            | 78.09                         | $4.88 \times 10^2$                             | 0.1065 |
|   | cat-800  | $y = -6900.92x - 8.01$   | 0.9630                            | 57.37                         | 22.94  | 0.1449 |
| 4 | cat-500  | $y = -9783.71x - 4.77$   | 0.9040                            | 81.34                         | $8.30 \times 10^{-2}$                          | 0.1022 |
|   | cat-800  | $y = -7211.33x - 7.60$   | 0.9623                            | 59.95                         | 36.12  | 0.1387 |
| 5 | cat-500  | $y = -10,185.39x - 4.25$ | 0.9013                            | 84.68                         | $1.45 \times 10^3$                             | 0.0982 |
|   | cat-800  | $y = -7529.78x - 7.18$   | 0.9614                            | 62.60                         | 57.39  | 0.1328 |

#### 4. Conclusions

This paper discussed the composition distribution and structure characteristics of the carbon deposited on the surface of the Ni- $\text{Al}_2\text{O}_3$  catalyst after a stability test for  $\text{CO}_2$  reforming of  $\text{CH}_4$ . The carbon deposition on the prepared catalyst is mainly composed of a filamentous one, whose accumulation in large amounts will block the catalyst pores and affect the catalyst performance. The area proportions of the first hydrogen consumption peaks of SCM and HTP at low temperatures ( $<350$  °C) account for 30–35%, higher than those of IMP and T310. Moreover, the area proportion of the low-temperature hydrogen consumption peak of T310 is as low as 9.79%, indicating that there is more inert carbon deposition on the surface of this catalyst. With respect to the  $\gamma$ -type carbon species, both T310 and HTP account for a high proportion, and their decarburization behavior directly affects the stability of the catalysts. According to the kinetic analysis based on the Coats–Redfern model, the fitting effect for different catalysts is not the same, and the suitable reaction order is also different. Obviously, the catalyst prepared at a higher calcination temperature shows lower carbon deposition, but a higher degree of graphitization after the reaction, which was not conducive to catalyst stability. A kinetic analysis based on the Coats–Redfern model presents that the decarburization temperature of each catalyst is mainly in the 500–700 °C temperature range and the decarburization activation energy is in the range of 50–80 kJ/mol.

**Author Contributions:** W.-L.M. designed the study, performed the research, analyzed data, and wrote the paper. Y.R. analyzed data and wrote the paper. Y.M. contributed to refining the ideas and carried out additional analyses. J.G. contributed to the writing and revisions. Z.-H.F. carried out additional analyses. S.-P.Z. discussed the results. X.-Q.Y. discussed the results. All authors have read and agreed to the published version of the manuscript.

**Funding:** Natural science foundation of Xinjiang Uyghur Autonomous Region (2022D01C23), Ningxia natural science foundation (2022AAC03307), special projects from Changji (2022Z04) and Xinjiang Uyghur Autonomous Region (ZYYD2022C16).

**Data Availability Statement:** Data is contained within the article.

**Conflicts of Interest:** The authors declare no conflict of interest.

## References

1. Liu, Q.; Wang, S.J.; Zhao, G.M.; Yang, H.Y.; Yuan, M.; An, X.X.; Zhou, H.F.; Qiao, Y.Y.; Tian, Y.Y. CO<sub>2</sub> methanation over ordered mesoporous NiRu-doped CaO-Al<sub>2</sub>O<sub>3</sub> nanocomposites with enhanced catalytic performance. *Int. J. Hydrog. Energy* **2018**, *43*, 239–250. [[CrossRef](#)]
2. Zainm, M.; Mohameda, R. An overview on conversion technologies to produce value added products from CH<sub>4</sub> and CO<sub>2</sub> as major biogas constituents. *Renew. Sustain. Energy Rev.* **2018**, *98*, 56–63. [[CrossRef](#)]
3. Lougou, B.G.; Shuai, Y.; Chaffa, G.; Xing, H.; Tan, H.; Du, H. Analysis of CO<sub>2</sub> utilization into synthesis gas based on solar thermochemical CH<sub>4</sub>-reforming. *J. Energy Chem.* **2019**, *28*, 61–72. [[CrossRef](#)]
4. Ruckenstein, E.; Wang, H.Y. Carbon deposition and catalytic deactivation during CO<sub>2</sub> reforming of CH<sub>4</sub> over Co/ $\gamma$ -Al<sub>2</sub>O<sub>3</sub> catalysts. *J. Catal.* **2002**, *205*, 289–293. [[CrossRef](#)]
5. Daza, C.E.; Gallego, J.; Mondragón, F.; Moreno, S.; Molina, R. High stability of Ce-promoted Ni/Mg-Al catalysts derived from hydrotalcites in dry reforming of methane. *Fuel Guildf.* **2010**, *89*, 592–603. [[CrossRef](#)]
6. Kawi, S.; Kathiraser, Y.; Ni, J.; Oemar, U.; Li, Z.; Saw, E.T. Progress in Synthesis of Highly Active and Stable Nickel-Based Catalysts for Carbon Dioxide Reforming of Methane. *ChemSusChem* **2015**, *8*, 3556–3575. [[CrossRef](#)] [[PubMed](#)]
7. Dux, J.; Zhang, D.S.; SHI, L.Y.; Gao, R.H.; Zhang, J.P. Coke- and sintering-resistant monolithic catalysts derived from in situ supported hydrotalcite-like films on Al wires for dry reforming of methane. *Nanoscale* **2013**, *5*, 2659–2663.
8. Wang, H.; Mo, W.; He, X.; Fan, X.; Ma, F.; Liu, S.; Tax, D. Effect of promoter on the structure, performance and carbon deposition of Ni-Al<sub>2</sub>O<sub>3</sub> catalyst for CO<sub>2</sub>-CH<sub>4</sub> reforming. *ACS Omega* **2021**, *6*, 16381–16390. [[CrossRef](#)] [[PubMed](#)]
9. Mo, W.L.; Ma, F.Y.; Liu, Y.E.; Liu, J.M.; Zhong, M.; Aisha, N. Effect of preparation method on the catalytic performance of Ni-Al<sub>2</sub>O<sub>3</sub> catalyst in CO<sub>2</sub>-CH<sub>4</sub> reforming reaction. *J. Fuel Chem. Technol.* **2015**, *43*, 1083–1091.
10. Guo, J.; Lou, H.; Zheng, X. The deposition of coke from methane on a Ni/MgAl<sub>2</sub>O<sub>4</sub> catalyst. *Carbon* **2007**, *45*, 1314–1321. [[CrossRef](#)]
11. Junke, X.U.; Wei, Z.H.; Jihui, W.A.; Zhaojing, L.I.; Jianxin, M.A. Characterization and analysis of carbon deposited during the dry reforming of methane over Ni/La<sub>2</sub>O<sub>3</sub>/Al<sub>2</sub>O<sub>3</sub> catalysts. *Chin. J. Catal.* **2009**, *30*, 1076–1084.
12. Frusteri, F.; Spadaro, L.; Arena, F.; Chuvilin, A. TEM evidence for factors affecting the genesis of carbon species on bare and K-promoted Ni/MgO catalysts during the dry reforming of methane. *Carbon* **2002**, *40*, 1063–1070. [[CrossRef](#)]
13. Cao, J.; Qiao, X.C.; Liu, C.L.; Zhang, J.S. Decomposition kinetics of limestone in mixed atmosphere of carbon dioxide and air. *Inorg. Salt Ind.* **2016**, *48*, 32–36.
14. Mow, L.; Maf, Y.; Liu, Y.E.; Liu, J.M.; Zhong, M.; Nulahonga, S. Effect of roasting temperature on the performance of NiO/ $\gamma$ -Al<sub>2</sub>O<sub>3</sub> catalyst for CO<sub>2</sub>-CH<sub>4</sub> reforming syngas. *J. Inorg. Mater.* **2016**, *31*, 234–240.

**Disclaimer/Publisher's Note:** The statements, opinions and data contained in all publications are solely those of the individual author(s) and contributor(s) and not of MDPI and/or the editor(s). MDPI and/or the editor(s) disclaim responsibility for any injury to people or property resulting from any ideas, methods, instructions or products referred to in the content.